Multi-transcriptome analysis following an acute skeletal muscle growth stimulus yields tools for discerning global and MYC regulatory networks

Kevin A. Murach

Zhengye Liu

Baptiste Jude

Vandre C. Figueiredo

Yuan Wen

See next page for additional authors

Authors

Kevin A. Murach, Zhengye Liu, Baptiste Jude, Vandre C. Figueiredo, Yuan Wen, Sabin Khadgi, Seongkyun Lim, Francielly Morena da Silva, Nicholas P. Greene, Johanna T. Lanner, John J. McCarthy, Ivan Jose Vechetti Jr, and Ferdinand von Walden

Multi-transcriptome analysis following an acute skeletal muscle growth stimulus yields tools for discerning global and MYC regulatory networks

Kevin A. Murach[1,2,*], Zhengye Liu[3], Baptiste Jude[3,4], Vandre C. Figueiredo[5,8], Yuan Wen[5,6], Sabin Khadgi[1], Seongkyun Lim[1,7], Francielly Morena da Silva[1,7], Nicholas P. Greene[1,2,7], Johanna T. Lanner[3], John J. McCarthy[5,8], Ivan J. Vechetti[9,*,‡], and Ferdinand von Walden[4,*,‡]

From the [1]Department of Health, Human Performance, and Recreation, Exercise Science Research Center, University of Arkansas, Fayetteville, Arkansas, USA, and [2]Cell and Molecular Biology Graduate Program, University of Arkansas, Fayetteville, Arkansas, USA; [3]Department of Physiology and Pharmacology, Karolinska Institute, Solna, Sweden, and [4]Department of Women's and Children's Health, Karolinska Institute, Solna, Sweden; [5]Center for Muscle Biology, University of Kentucky, Lexington, Kentucky, USA, and [6]Department of Physical Therapy, University of Kentucky, Lexington, Kentucky, USA; [7]Cachexia Research Laboratory, University of Arkansas, Fayetteville, Arkansas, USA; [8]Department of Physiology, University of Kentucky, Lexington, Kentucky, USA; [9]Department of Nutrition and Health Sciences, University of Nebraska-Lincoln, Nebraska, USA

Edited by Enrique De La Cruz

Myc is a powerful transcription factor implicated in epigenetic reprogramming, cellular plasticity, and rapid growth as well as tumorigenesis. Cancer in skeletal muscle is extremely rare despite marked and sustained *Myc* induction during loading-induced hypertrophy. Here, we investigated global, actively transcribed, stable, and myonucleus-specific transcriptomes following an acute hypertrophic stimulus in mouse plantaris. With these datasets, we define global and *Myc*-specific dynamics at the onset of mechanical overload-induced muscle fiber growth. Data collation across analyses reveals an under-appreciated role for the muscle fiber in extracellular matrix remodeling during adaptation, along with the contribution of mRNA stability to epigenetic-related transcript levels in muscle. We also identify *Runx1* and *Ankrd1* (*Marp1*) as abundant myonucleus-enriched loading-induced genes. We observed that a strong induction of cell cycle regulators including *Myc* occurs with mechanical overload in myonuclei. Additionally, *in vivo Myc*-controlled gene expression in the plantaris was defined using a genetic muscle fiber-specific doxycycline-inducible *Myc*-overexpression model. We determined *Myc* is implicated in numerous aspects of gene expression during early-phase muscle fiber growth. Specifically, brief induction of *Myc* protein in muscle represses *Reverbα*, *Reverbβ*, and *Myh2* while increasing *Rpl3*, recapitulating gene expression in myonuclei during acute overload. Experimental, comparative, and *in silico* analyses place *Myc* at the center of a stable and actively transcribed, loading-responsive, muscle fiber–localized regulatory hub. Collectively, our experiments are a roadmap for understanding global and *Myc*-mediated transcriptional networks that regulate rapid remodeling in postmitotic cells. We provide open webtools for exploring the five RNA-seq datasets as a resource to the field.

Myc is a transcription factor known to drive cellular plasticity (1, 2), epigenetic reprogramming toward stemness as a Yamanaka factor (3–6), and rapid growth *via* proliferative and nonproliferative mechanisms (7–9). A proto-oncogene that dimerizes with MAX and interacts and/or complexes with numerous other proteins, (10, 11) MYC protein is a "universal amplifier" and "supermanager" of transcription with intricate and multifaceted functionality (12–14). Evidence for a role of MYC in syncytial muscle fiber growth emerged 20 to 30 years ago (15–17). A decade ago, MYC was hypothesized to be a key aspect of skeletal muscle adaptation to exercise (18). We recently found that the promoter region of *Myc* was hypomethylated in myonuclei following short-term mechanical overload of the mouse plantaris muscle (19). MYC protein binds the ribosomal DNA promoter during muscle overload (20), consistent with its influence on ribosome biogenesis and protein synthesis in striated muscle (21, 22). We also report that MYC-associated areas of ribosomal DNA are differentially methylated in murine myonuclei and human muscle tissue after acute loading (23). Dysregulation of *Myc* results in tumor development and maintenance in mononuclear cells (8, 9). Even transiently elevated MYC can cause tumors in some cells (24); however, *Myc* transcript and protein (MYC) may be elevated for up to 2 weeks during continuous mechanical overload in mouse muscle without an overt deleterious effect (23, 25–28). MYC protein abundance in human muscle after resistance training also associates with the magnitude of hypertrophic adaptation (29). The unique multinuclear, terminally differentiated postmitotic nature of muscle fibers likely explains how muscle is resistant to developing cancer (30–33) and why sustained MYC is tolerated in this tissue. Although the role of MYC in proliferative cells is well studied, its

function as a transcription factor in postmitotic myonuclei during muscle growth is incompletely defined.

In the current investigation, we generated four interrelated murine muscle RNA-sequencing (RNA-seq) datasets using a proven hypertrophic loading stimulus (34, 35) to understand muscle tissue and myonucleus-specific transcriptional dynamics at the onset of rapid muscle growth. We focused on the effects of *Myc* given its (1) established role in driving non-proliferative tissue growth and overall cellular plasticity in nonmuscle cell types (1, 7) and (2) proposed role in human (23, 29, 36) and rodent (17, 20, 22, 25–28) loading-induced skeletal muscle hypertrophy. We then performed a genetically driven muscle fiber–specific *in vivo Myc* overexpression experiment along with *in silico* chromatin immunoprecipitation sequencing (ChIP-seq) analysis to provide focused insight on how *Myc* may contribute to global gene expression during rapid muscle remodeling.

Results

Figure 1*A* is a study design schematic. *Experiment 1* defines the global transcriptome using RNA-seq after 72 h of synergist ablation mechanical overload of the mouse plantaris muscle. *Experiments 2 and 3* used the tissue from *Experiment 1* to provide information on the contribution of active transcription *versus* mRNA stability to global gene expression with overload. *Experiment 4* details the myonucleus-specific transcriptome during overload to identify muscle fiber–enriched genes, which is further informed by *Experiments 2 and 3*. Myonuclei only comprise ∼30% of all nuclei after short-term mechanical overload (19), so defining the transcriptome specifically in myonuclei is critical for understanding muscle fiber adaptation. The transcriptional regulation and localization of *Myc* and its impact on muscle gene expression were explored using data from *Experiments 1 to 4*. *Experiment 5* utilized a doxycycline-inducible muscle fiber–specific *in vivo Myc* pulse
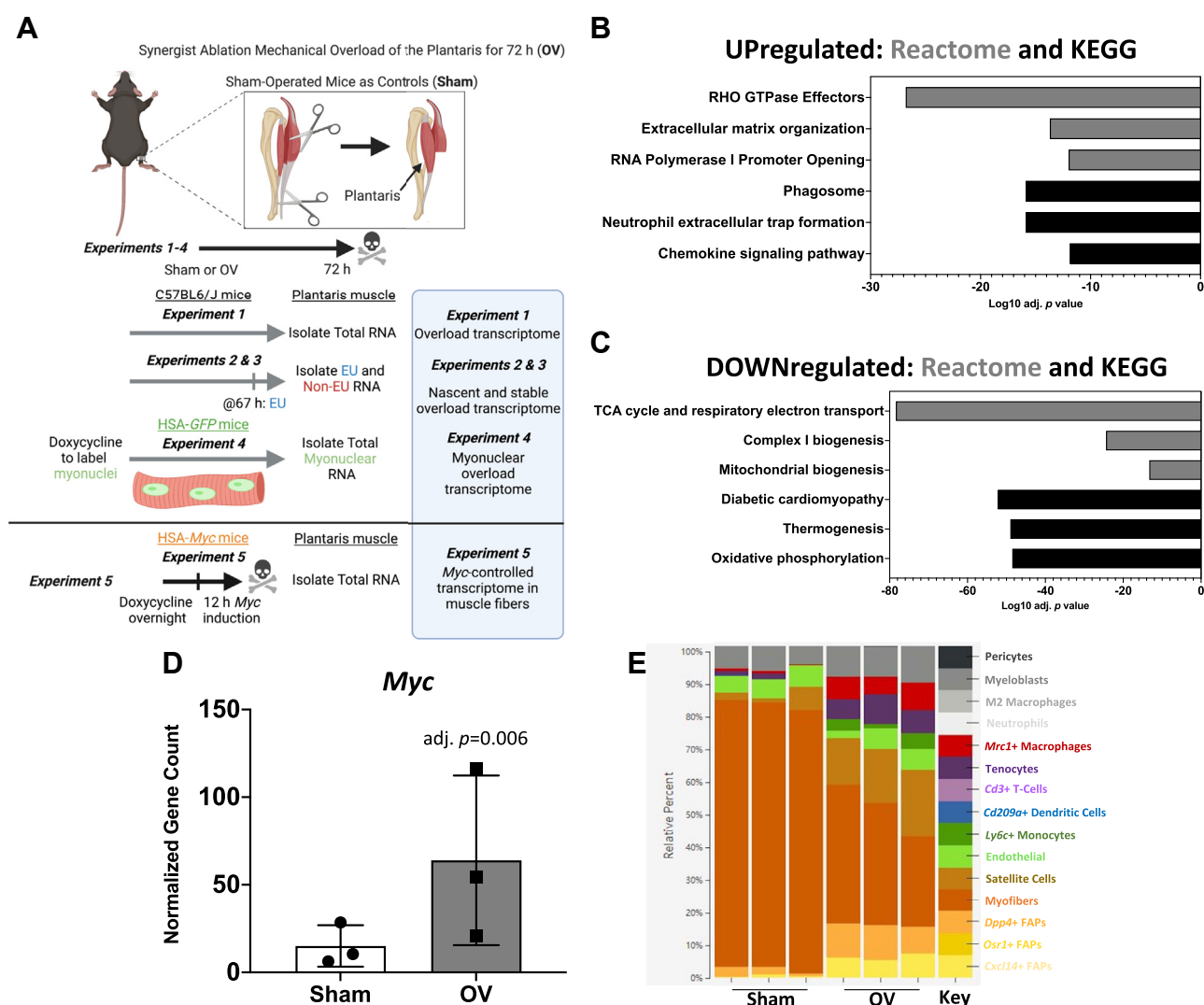
Figure 1. *Experiment 1*: RNA-sequencing of total RNA from plantaris muscle after 72 h of mechanical overload. *A*, study design schematic showing the conditions of *Experiments 1 to 5*. *B*, pathway analysis of upregulated genes in OV *versus* sham. *C*, pathway analysis of downregulated genes in OV *versus* sham. *D*, *Myc* mRNA levels in sham and overload determined by RNA-seq. *E*, digital deconvolution of muscle overload data using CIBERSORTx (42) and data from Oprescu *et al.* (43) to delineate cellular contributions to the global transcriptome. Normalized gene count, gene counts normalized using DESeq2. EU, 5-Ethenyl uridine; OV, overload.

in the plantaris to understand what genes *Myc* controls within muscle fibers and how this relates to myonuclear gene expression during overload (*Experiment 4*); we corroborated the results from these analyses using computational ChIP-seq (37). All transcriptome data are publicly available for browsing:

Experiments 1 to 3 https://liuzhengye.github.io/Hypertrophy/interactive_MA_PLOT_Eu.html

Experiment 4 https://liuzhengye.github.io/Hypertrophy/interactive_MAplot_myonuclei.html

Experiment 5 https://liuzhengye.github.io/Hypertrophy/interactive_MA_MYC.html

Experiment 1: The global plantaris transcriptome after 72 h of mechanical overload

Pathway analysis of differentially regulated genes (false discovery rate adjusted *p* value [adj. *p*] < 0.05) in plantaris tissue after overload revealed extracellular matrix (ECM), inflammatory, histone (RNA Pol I), and RHO-GTPase gene expression were higher relative to sham (Fig. 1*B*) (Table S1 and S2). A large proportion of downregulated genes were related to oxidative metabolism (Fig. 1*C*) (Table S3). This repressed gene signature could contribute to a "Warburg effect" that occurs during rapid overload-induced muscle hypertrophy, marking a shift toward "aerobic glycolysis" for rapid biomass accumulation (38–41). Consistent with our prior murine studies (19, 25, 26) and human resistance exercise time course data (23), *Myc* was higher after overload (Log2FC = 2.0, adj. *p* = 0.006) (Fig. 1*D*).

To provide insight on what cell types contribute to global gene expression profiles in sham and overload, we conducted digital deconvolution analysis with CIBERSORTx using *Experiment 1* transcriptome data (42). The analysis algorithm was trained using single cell RNA-seq data from a 10 days muscle regeneration dataset (43) (Fig. 1*E*). The interstitial cell proportion in muscle increases at the onset of overload, outnumbering myonuclei (19). Despite this shift, the largest contribution to gene expression in muscle was predicted to be from muscle fibers (*i.e.*, myonuclei) after 72 h of overload. The second largest contributions were from muscle stem cells (satellite cells) and fibro-adipogenic progenitors (Fig. 1*E*). We recently reported that successful ECM remodeling during the first 96 h of overload determines the long-term hypertrophic response (44). Early stage ECM remodeling is strongly influenced by satellite cells and fibro-adipogenic progenitors (44, 45); it follows that these cell types are major contributors to early-phase gene expression during growth.

Experiments 2 and 3: Nascent and stable mRNA transcriptomes after 72 h of mechanical overload

Most transcription in skeletal muscle is rRNA (46), and rRNA levels are further augmented specifically in myonuclei during overload (25). We conducted mRNA profiling to understand global transcriptional dynamics in the non-rRNA pool during growth using 5-Ethenyl uridine (EU) metabolic labeling (25) (Tables S4–S9). In the EU (nascent, *Experiment 2*) and non-EU (not actively transcribed and presumably stable, *Experiment 3*) mRNA fractions, ECM remodeling was

among the most upregulated processes during the last 5 h of overload *versus* sham (Fig. 2, *A* and *B*) (Tables S4–S6, and S8). *Myc* was also significantly higher in nascent and stable fractions relative to sham (Fig. 2*C*). Active *Myc* transcription during overload could be facilitated by hypomethylation of its promoter in myonuclei (19). Thus, ECM and *Myc* gene expression are highly regulated during the acute phase of muscle loading. In addition, RHO-GTPase genes were higher in both fractions with overload relative to sham (Fig. 2, *A* and *B*). RHO-GTPases are implicated in muscle mass regulation, but their role in load-induced hypertrophy is still being defined (47). Genes related to epigenetic control of gene expression (specifically histones and *Dnmt1*) were enriched in the non-EU fraction with overload (Fig. 2, *D* and *E*). Myonuclear histone turnover (48) and dynamic regulation of DNA methylation in myonuclei (19, 23, 49) likely facilitates hypertrophic gene expression and adaptation in muscle fibers.

In the EU and non-EU fractions, oxidative metabolism-related gene expression was lower during overload (Fig. 2, *F* and *G*) (Tables S7 and S9); these data inform the findings from *Experiment 1*. *Pgc1α* (*Ppargc1a*), a core regulator of mitochondrial biogenesis (50, 51), was among genes that were lower in both fractions during overload (Tables S4 and S5). Apart from epigenetic-related genes, most mRNA differences between sham and overload at the pathway level were attributable to differences in both nascent transcription and, presumably, enhanced mRNA stability.

Experiment 4: The myonuclear transcriptome after 72 h of mechanical overload

To understand what genes were specifically regulated in muscle fibers during rapid muscle growth, we conducted RNA-seq on fluorescent activated nuclear-sorted (FANS)-purified myonuclei using the HSA-*GFP* mouse (Fig. 3*A*) (19, 52). Relative to sham, genes related to ECM remodeling (primarily collagens, matrix metalloproteinases, and secreted factors) and immune signaling (namely chemokines) were most highly enriched in myonuclei from overloaded muscle (Fig. 3*B*) (Tables S10 and S11). We and others have reported that matrix metalloproteinase 9 (*Mmp9*) is responsive to loading in skeletal muscle and is a key component of muscle growth (53–55). We confirm here that *Mmp9* is enriched in myonuclei during overload *in vivo* (Fig. 3*C*). Interstitial cells of the muscle microenvironment are generally viewed as the primary contributors to ECM deposition and turnover. Emerging evidence suggests that muscle fibers also play a major role in ECM remodeling (53, 56–58), which the current data reinforces.

Numerous cell cycle regulators were enriched in myonuclei after overload (Fig. 3*B*) which included *Myc* (top 30 upregulated gene, adj. *p* = 0.0136×10^{-7}) (Fig. 3*C*) (Table S11). *Runx1*, another transcription factor, was highly abundant and enriched in myonuclei by overload (Log2FC = 4.1, adj. *p* = 0.05×10^{-14}) (Fig. 3*E*); it was also markedly higher in total RNA, EU, and non-EU fractions (Tables S1, S4 and S5). *Runx1* induction during overload is intuitive since it regulates muscle
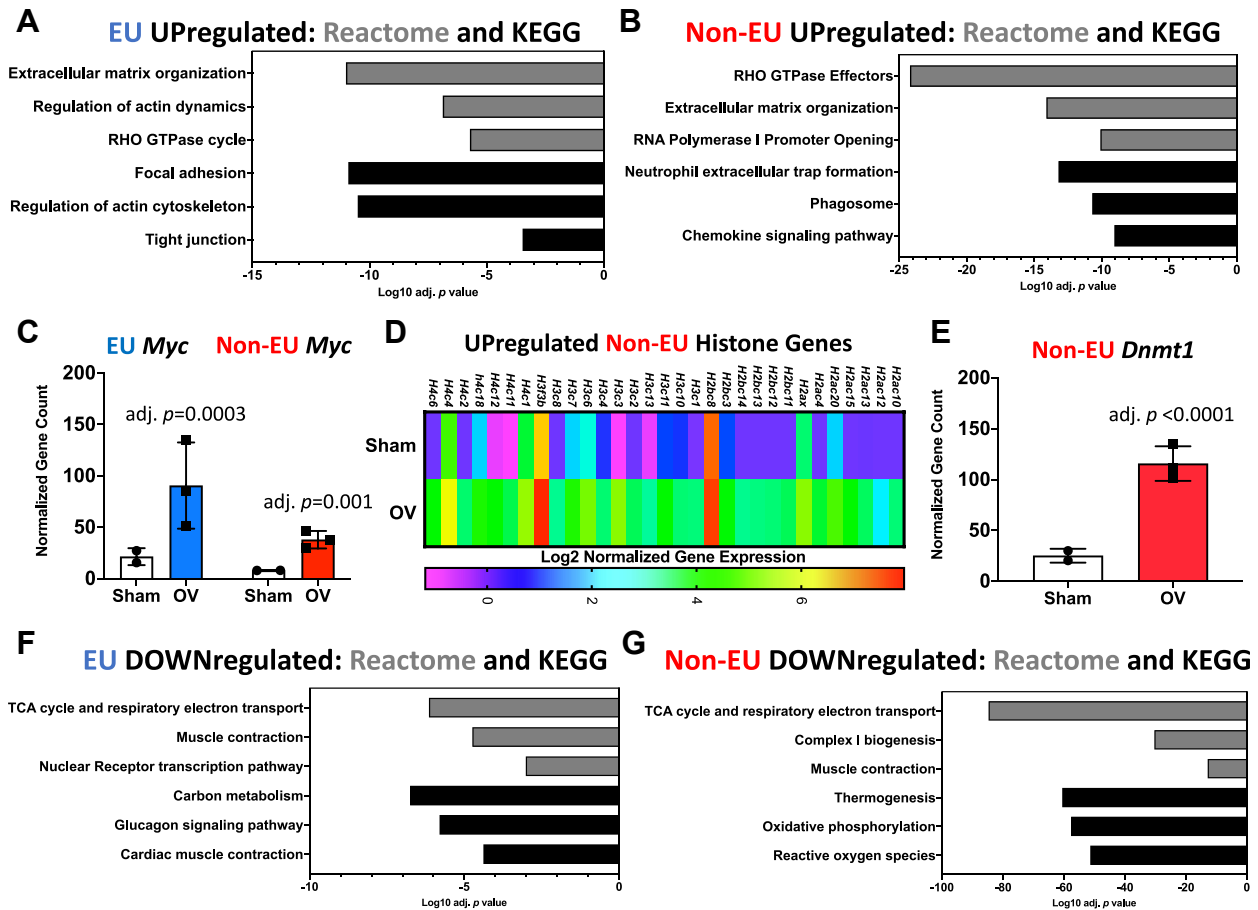
Figure 2. *Experiments 2 and 3*: RNA-sequencing of EU- and Non-EU–labeled mRNA from plantaris after 72 h of mechanical overload. *A*, pathway analysis of genes upregulated in the EU-labeled fraction in OV *versus* sham. *B*, pathway analysis of genes upregulated in the Non-EU–labeled fraction in OV *versus* sham. *C*, *Myc* mRNA levels in the EU and Non-EU fractions. *D*, histone genes elevated in the Non-EU fraction during overload. *E*, *Dnmt1* mRNA levels in EU and Non-EU fractions. *F*, pathway analysis of genes downregulated in the EU-labeled fraction in OV *versus* sham. *G*, pathway analysis of genes downregulated in the Non-EU–labeled fraction in OV *versus* sham. EU, 5-Ethenyl uridine; OV, overload.

mass, myofibrillar organization, and autophagy in myofibers (59). RUNX1 is also known to interact and complex with MYC (60, 61). *Ankrd1* (*Marp1*, also *Carp1*) was the most upregulated gene with overload in myonuclei (Log2FC = 6.0, adj. *p* = 0.0127×10^{-62}) as well as the EU fraction (Log2FC = 5.1, adj. *p* = 0.038×10^{-60}) (Fig. 3*F*) (Tables S4, S5, and S10); however, it was only the 1495th most differentially regulated gene in the total RNA dataset (Table S1). *Ankrd10* was also among the most upregulated genes in myonuclei and the EU fraction. *Ankrd1* localizes in myotendinous junction myonuclei (62) and is induced by eccentric exercise in rodent and human muscle (63, 64). Perhaps *Ankrd1* upregulation during mechanical overload is partially explained by muscle lengthening and/or myotendinous junction remodeling (35, 65). These results highlight the power of EU-labeling and myonucleus-specific transcriptomics for identifying potentially important genes for muscle growth. Our findings also provide impetus for further investigation of *Ankrd1* during muscle hypertrophy. The category of genes most downregulated during overload in myonuclei was oxidative metabolism (Fig. 3*G*) (Table S12). Thus, the total mRNA and EU results are likely driven by changes within the myofiber.

Experiment 5: The Myc-controlled transcriptome in plantaris muscle fibers

We generated a doxycycline-inducible HSA-*Myc* mouse to experimentally define the MYC regulatory network in plantaris muscle fibers. A pulse of *Myc* was driven *via* doxycycline in water overnight followed by a 12-h period without doxycycline. Principal component analysis revealed stark differences between control and *Myc* overexpression (Fig. 4*A*). At the pathway level, ribosome biogenesis-related genes such as ribosomal proteins and eukaryotic initiation factors were most upregulated relative to controls (Fig. 4*B*) (Table S13). A MYC pulse induced gene expression of the large ribosomal subunit protein *Rpl3* (Log2FC = 1.95, adj. *p* = 0.00053) (Fig. 4*C*). *Rpl3* was also higher in myonuclei during overload, and its muscle-specific paralog *Rpl3l* was lower (adj. *p* < 0.05) (Table S10). Upregulation of *Rpl3* has been implicated in robust hypertrophy in mouse (26) and human muscle (29). *Rpl3* may influence growth *via* ribosome specialization (66), but more work is needed in this area. The induction of *Rpl3* by overload and *Myc* alongside increased levels of the rRNA transcription-associated genes *Bop1* (67, 68), *Ftsj3* (69), *Polr3g* (70), *Rpl10a* (71), and *Rps19* (72), could also be a sign of enhanced
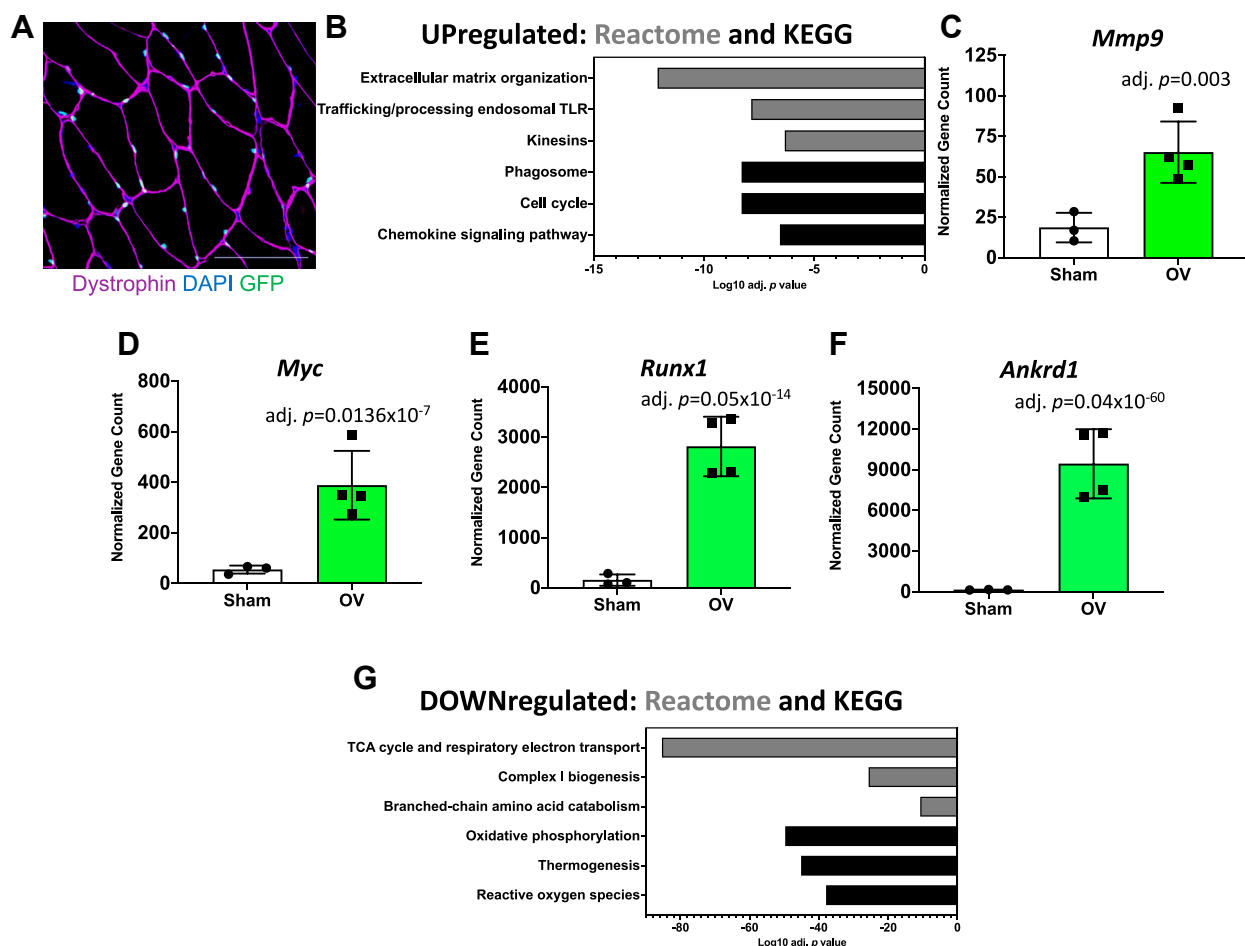
Figure 3. *Experiment 4*: **RNA-sequencing of myonuclear RNA from plantaris muscle after 72 h of mechanical overload.** *A*, image showing myonuclear GFP labeling, DNA (DAPI), and dystrophin *via* histochemistry in a doxycycline-treated HSA-*GFP* mouse (see refs. (19) and (99)); the scale bar represents 100 μm. *B*, pathway analysis of upregulated genes specifically in FANS-isolated myonuclei in OV *versus* sham. *C*, myonuclear *Mmp9* mRNA levels in sham and overload determined by RNA-seq. *D*, *Myc* mRNA levels in sham and overload determined by RNA-seq. *E*, *Runx1* mRNA levels in sham and overload determined by RNA-seq. *F*, *Ankrd1* (*Marp1*) mRNA levels in sham and overload determined by RNA-seq. *G*, pathway analysis of downregulated genes specifically in FANS-isolated myonuclei in OV *versus* sham. FANS, fluorescent activated nuclear-sorted; OV, overload.

ribosome biogenesis. In total, 31 upregulated genes were common to *Myc* overexpression in muscle fibers and myonuclei with overload (Fig. 4*D*).

Approximately, 100 genes were downregulated (adj. $p <$ 0.05) by MYC in the plantaris (Table S13). MYC strongly regulates microRNA expression (8, 73–77). Repressed genes with MYC induction are potentially attributable to MYC-controlled microRNA-mediated mRNA destabilization and degradation. MYC may also repress gene expression *via* regulating DNA methylation and chromatin remodeling (3, 4, 12), as well as through specific protein-protein interactions (10, 11). The abundant myosin heavy chain type 2a gene *Myh2* was repressed by MYC (Log2FC = −0.75, adj. p = 0.013) (Fig. 4*E*), similar to what occurred in myonuclei during overload (Table S10). Type 2a myosin is associated with oxidative metabolism in murine muscle (78, 79). Lower *Myh2* may be part of a Warburg-like program that accompanies rapid muscle growth (38, 39). *Reverbα* (*Nr1d1*, Log2FC = −1.36, adj. p = 0.065) and *Reverbβ* (*Nr1d2*, Log2FC = −1.31, adj. p = 0.044) mRNA levels were lower with MYC overexpression (Fig. 4*F*) and in myonuclei with overload (Table S10). In cancer

cells, MYC promotes *Reverbα* and *Reverbβ* expression (80) which affects the core clock gene *Bmal1* (80, 81), circadian rhythm, and cell metabolism (80). Thus, MYC control of *Reverb*s could be unique in muscle fibers. In total, 35 downregulated genes were common to MYC overexpression in muscle fibers and myonuclei with overload (Fig. 4*G*).

To corroborate MYC regulation of target genes in muscle, we compared our overload myonuclear and *Myc* overexpression RNA-seq data to published MYC ChIP-seq data from myogenic cells (77). Of genes regulated by both overload and MYC (Fig. 4, *D* and *G*), *Anp32b, Aqp4, Atp1a1, Cdkn1b, Cntfr, Epas1, Ftsj3, Jak2, Ncl, Nr1d2/Reverbβ, P2ry1, Pcmtd1, Rpl3,* and *Slc7a5* featured MYC occupancy in myogenic cells. After differentiation, MYC-binding peaks on all these genes except *Aqp4, Atp1a1,* and *P2ry1* were altered, indicating regulation by MYC in dynamic conditions. Of note, MYC binding to *Ankrd1* increased during myotube formation (77). Brief *Myc* overexpression in the soleus did not induce *Ankrd1*, so MYC may function cooperatively with another factor that is induced during overload to regulate this gene (14, 82). To confirm MYC transcription factor binding of myonuclear
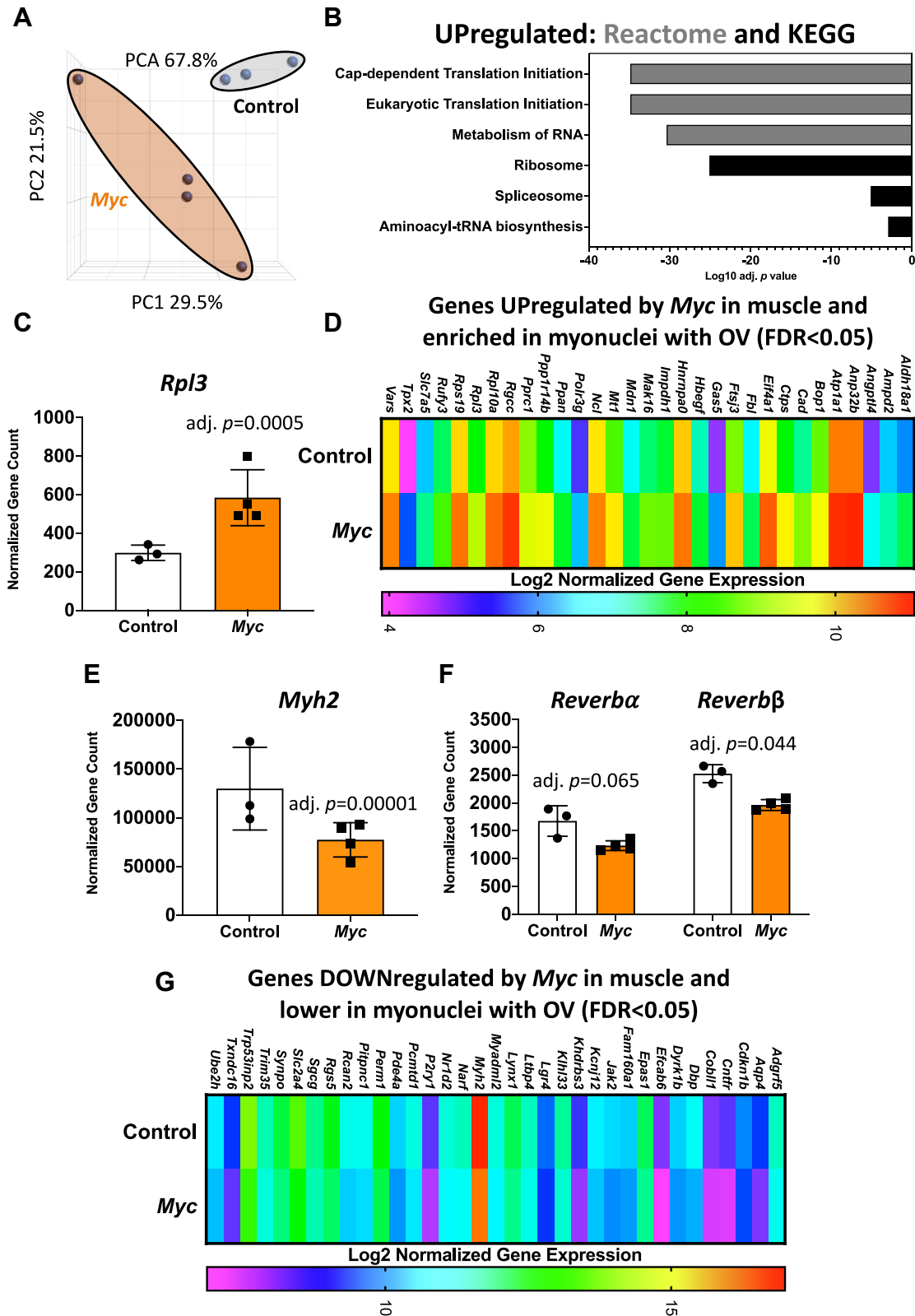
Figure 4. *Experiment 5*: RNA-sequencing of total RNA from plantaris muscle of HSA-*Myc* mice following a single pulse of *Myc*. *A*, PCA plots from doxycycline-treated HSA-*Myc versus* littermate HSA-*rtTA* (Control) mice (generated using DESeq2 normalized gene counts). *B*, pathway analysis of upregulated genes after *Myc* overexpression. *C*, *Rpl3* mRNA levels after *Myc* overexpression. *D*, genes upregulated by *Myc* in muscle and also enriched in myonuclei during 72 h of overload. *E*, *Myh2* mRNA levels after *Myc* overexpression. *F*, *Reverbα* (*Nr1d1*) and *Reverbβ* (*Nr1d2*) after *Myc* overexpression. *G*, genes upregulated by *Myc* in muscle also enriched in myonuclei during 72 h of overload. OV, overload; PCA, principal component analysis.

DNA during mechanical overload, we utilized our RNA-seq data to perform epigenetic Landscape *In Silico* deletion Analysis (Lisa) (37). Lisa incorporates transcriptome input data with an extensive library of publicly available transcription factor ChIP-seq and global chromatin accessibility profiles to infer transcriptional regulators. Leveraging our MYC over-expression RNA-seq data as a control (*Experiment 5*), MYC/MYCN was the highest ranked transcription factor driving upregulated genes (Table S14), confirming the accuracy of Lisa. Using the first 500 differentially regulated genes in each direction from *Experiment 4*, MYC was in the top 5% of transcription factors controlling upregulated genes ($p = 1.7 \times 10^{-24}$) in myonuclei during overload and the top 10% for controlling downregulated genes ($p = 2.4 \times 10^{-11}$) (Table S15). Motif target prediction suggested that MYC regulates *Rpl3* in myonuclei during overload (top 45% of genes targeted by

MYC) (Table S16). Ribosome biogenesis-associated *Bop1* (top 15%), *Ftsj3* (top 15%), *Polr3g* (top 1%), and *Rps19* (top 15%) had high regulatory potential by MYC during overload according to H3k27ac ChIP-seq (promoter/enhancer) information; *Ncl* was also in the top 1% (Table S17). MYC had regulatory potential for *Nr1d2/Reverbβ* during overload (top 35% of gene targets) (Table S18). All together, these data suggest that MYC controls gene expression in myonuclei during loading-induced hypertrophy.

Discussion

Interrelated RNA-seq datasets define the early phase of growth processes in differentiated muscle fibers (Fig. 5). Lower oxidative metabolism-related gene expression during the onset of rapid muscle growth is due to changes in mRNA
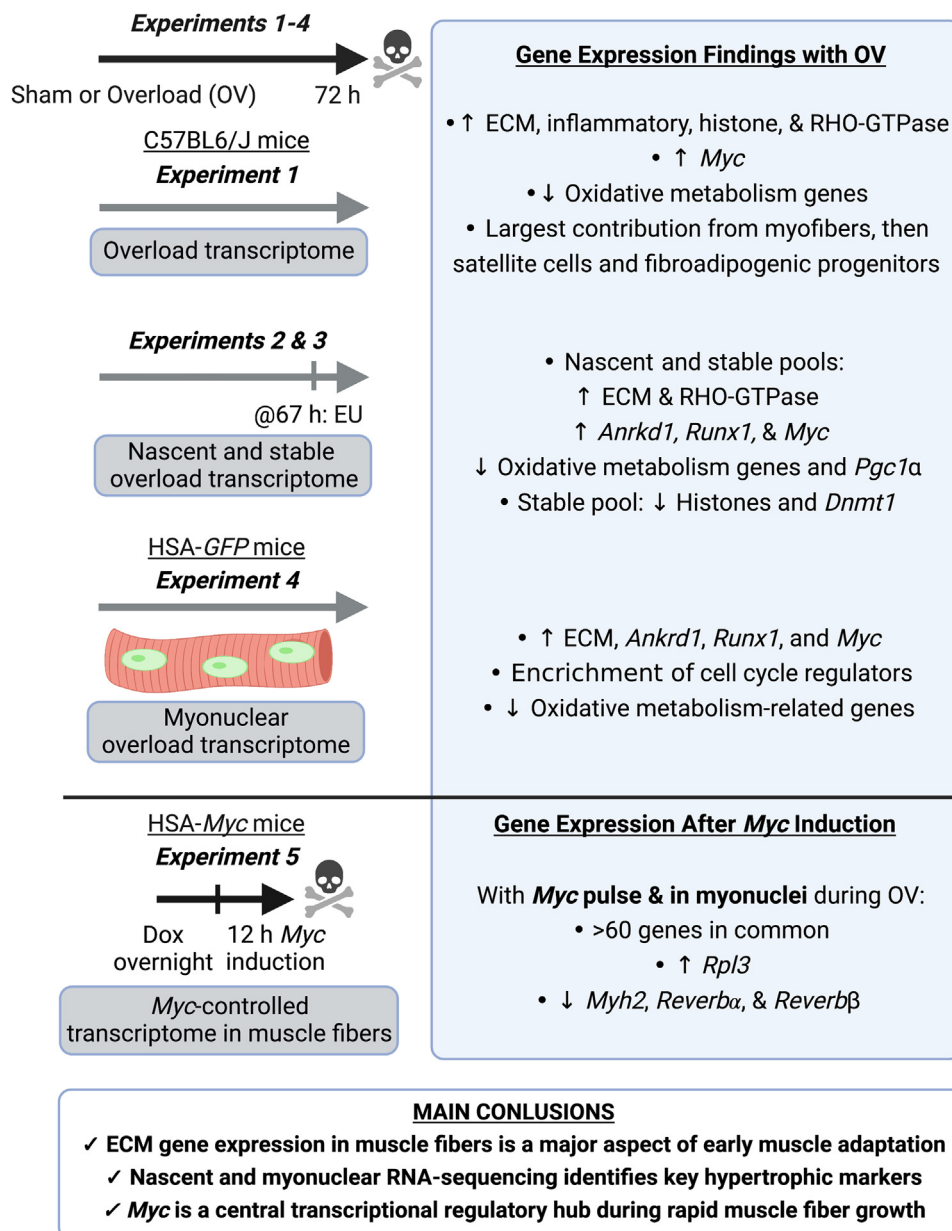

Figure 5. Summary of key findings from *Experiments 1 to 5*.

transcription and stability and occurs specifically in myonuclei. The overload datasets also revealed an under-appreciated role for muscle fibers in ECM remodeling during adaptation. Regulation of several collagens and remodeling enzymes such as *Mmp*s by active transcription, transcript stability, and in myonuclei emphasizes the importance of ECM dynamics for muscle hypertrophy (56). The non-EU RNA-seq data suggests elevated epigenetic-related gene expression during overload reflects greater mRNA stability; the mechanism underlying the change in mRNA stability in muscle during hypertrophy deserves further investigation. We identified key genes that are actively transcribed in muscle and enriched in myonuclei during *in vivo* muscle growth, such as *Runx1* and *Ankrd1*. RUNX1 regulates muscle mass (59) and participates in ribosome biogenesis (83), as well as interacts with MYC (60, 61). ANKRD1 associates with titin's N2A element, a major mechanosensory and signaling hub in skeletal muscle (84, 85). It also locks titin to the thin filament, regulates passive force, and protects the sarcomere from mechanical damage (86). Some evidence suggests ANKRD1 inhibits TNFα-induced NFκB signaling (87) and affects androgen receptor signaling (88) in myogenic cell culture. Given these functions, ANKRD1 may be critical for successful muscle hypertrophy. *Ankrd1* was not among the most differentially expressed genes in the total RNA dataset but emerged in the nascent and myonuclear RNA-seq as the most highly responsive gene to mechanical overload. This mismatch highlights the utility of evaluating transcriptional dynamics and myonuclear-specific gene expression for understanding muscle adaptation. Furthermore, *Runx1* and *Ankrd1* are typically upregulated after muscle denervation (59, 87), suggesting a compensatory response to counteract atrophy in that condition.

MYC protein localizes in myonuclei during loading-induced skeletal muscle growth (15, 27). Genetic *Myc* induction recapitulates diverse aspects of the loading response in muscle fibers. These changes include downregulation of *Reverbα*, *Reverbβ*, and *Myh2*, along with increased *Rpl3*. Published ChIP-seq data in myogenic cells (77) as well as *in silico* transcriptional regulator analysis (37) using our myonuclear RNA-sequencing data corroborates the association of MYC with *Reverbβ* and *Rpl3*, along with numerous other genes. The ChIP-seq also revealed a potential interaction with *Ankrd1* (77) that did not emerge in our muscle-specific MYC overexpression experiment. Lower levels of *Reverb*s during overload could have implications for circadian regulation and metabolism in muscle fibers (80); this is salient since MYC is exercise-responsive and exercise shifts the circadian rhythm in skeletal muscle (89–92). Perhaps an exercise-mediated shift in muscle circadian rhythm is controlled by MYC, but more work is needed in this area, especially with respect to resistance exercise. Altered *Rpl3* by mechanical overload and MYC expression could facilitate muscle-specific growth *via* ribosome specialization (66, 93). MYC is also known to be a potent driver of ribosome biogenesis in muscle (21, 22). We previously reported that ribosome biogenesis increases in total and nascent RNA pools following 72 h of synergist ablation in the mouse (20, 23, 25, 94). Thus, MYC appears central to the

regulation of rRNA synthesis and ribosome assembly, processes hypothesized to be necessary for sustained hypertrophy in response to loading (95–97). MYH2 protein and oxidative fiber proportion increases after prolonged muscle overload (98). MYC-mediated and early *Myh2* downregulation during overload may relate to an acute glycolytic preference during rapid hypertrophy (38).

The induction of MYC in instances of attenuated muscle plasticity such as aging, where MYC activity may be blunted during hypertrophy (15), could restore adaptive potential and increase muscle mass. Future experiments involving simultaneous muscle-specific inducible knockout of *c-Myc* and its several analogous family members (99), myonuclear MYC ChIP-seq, and MYC protein–protein interactome analysis during overload will provide more granular insight on the MYC regulatory network during muscle hypertrophy. Since differentiated myofibers can sustain high levels of oncogene expression without tumor formation, we suggest that MYC in muscle fibers induced by loading is a core component of rapid yet functional adaptive remodeling. Collectively, our data are a rich resource for understanding transcriptional dynamics and MYC regulation during the onset of loading-induced muscle fiber growth.

Experimental procedures

Animals and animal procedures

All animal procedures were approved by the University of Kentucky and the University of Arkansas IACUC. Mice were housed in a temperature and humidity-controlled room, maintained on a 14:10-h light-dark cycle, and food and water were provided *ad libitum* throughout experimentation. Animals were sacrificed *via* a lethal dosage of sodium pentobarbital injected intraperitoneally or CO_2 asphyxiation followed by cervical dislocation.

Female C57BL6/J mice were obtained from the Jackson Laboratory for *Experiments 1 to 3*. Female HSA-rtTA$^{+/-}$;TRE-H2B-GFP$^{+/-}$ (HSA-*GFP*) mice were generated as previously described by us (19, 52) for *Experiment 4*. The TRE-H2B-GFP mouse was originally obtained from the Jackson Laboratory (005104, bred to homozygosity by our laboratory) (100). For *Experiment 5*, male HSA-rtTA$^{+/-}$;TRE-Myc$^{+/-}$ (HSA-*Myc*) were generated by crossing homozygous HSA-*rtTA* mice (52) with heterozygous TRE-*Myc* mice (101); HSA-*rtTA* littermate mice were used as controls. All mice were genotyped as described (52, 102). HSA-*GFP* mice were treated with low-dose doxycycline (0.5 mg/ml doxycycline in drinking water with 2% sucrose) for 5 days to label myonuclei with GFP. HSA-*Myc* and littermate control mice were treated with doxycycline water overnight, and this water was replaced with unsupplemented water for 12 h prior to being euthanized. All mice were at least 2 months of age at the time of experimentation.

For *Experiments 1 to 4*, synergist ablation overload of the plantaris was performed as described (19, 34). Synergist ablation involves removal of ~50% of the gastrocnemius–soleus complex while under anesthesia, followed by ambulatory cage behavior for 72 h. Sham surgery (control condition)

involved all the steps of synergist ablation but without removal of muscle. For *Experiments 1 to 3*, mice were injected with EU 5 h prior to being euthanized (25). Briefly, mice were given an intraperitoneal injection of 2 mg of EU (Jena Biosciences) suspended in sterile PBS. For *Experiment 4*, myonuclei were isolated *via* FANS (19). Plantaris muscles were harvested immediately after being euthanized. Muscle was minced and homogenized *via* Dounce in a sucrose buffer with RNAse inhibitors. After straining through 40 μm filters, the nuclear suspension was pulsed with propidium iodide to label DNA. GFP+/PI+ myonuclei were sorted using FANS into TRIzol LS for RNA isolation.

RNA isolation and sequencing

For *Experiments 1*, *2*, *3*, and *5*, plantaris RNA was isolated using TRI Reagent (Sigma-Aldrich). Tissue was homogenized using beads and the Bullet Blender Tissue Homogenizer (Next Advance) or the Fisher Bead Mill (Fisher). Following homogenization, RNA was isolated *via* phase separation by addition of bromochloropropane or chloroform and then by centrifugation. The aqueous phase was transferred to a new tube and further processed on columns using the Direct-zol Kit (Zymo Research) (23). For *Experiment 4*, RNA was isolated by Norgen. *Experiments 1*, *4*, and *5* utilized Poly-A enrichment. For *Experiments 2* and *3*, RNA was depleted of rRNA using the NEBNext rRNA Depletion Kit (New England Biolabs) prior to isolation of EU- and non-EU–labeled RNA. A total of 4×1 μg RNA reactions were used per sample for rRNA depletion and pooled for the EU pulldown. The EU- and non-EU–labeled RNA fractions were isolated using the Click-iT Nascent RNA Capture kit (ThermoFisher) per the manufacturers protocol. cDNA libraries were constructed using NEBNext Ultra# II RNA Library Prep kit with NEBNext Multiplex Oligos for Illumina (New England Biolabs). EU pulldowns were unsuccessful for one sham experiment, so sequencing for that group was n = 2. Library preparation for *Experiment 4* was low input and utilized the SMARTer pico kit (TaKaRa), as described by the National Genomics Infrastructure at SciLifeLab. RNA for *Experiments 1*, *2*, *3*, and *5* were sequenced by Novogene on an Illumina HiSeq using 150 bp paired-end sequencing, as we have done previously (79, 103). *Experiment 4* was sequenced by the SciLifeLab on a NovaSeq 6000 (150 bp paired-end).

Transcriptomic analyses

Raw counts from RNA-seq were used as inputs into R (Version 4.1.0) or Partek Flow. Alignment was performed using STAR with mmu39. After filtering low-expressed genes, *DESeq2* (Version 1.34.0) was used for normalization and differential analyses of RNA-seq data to identify differentially expressed genes (DEGs) with pairwise comparisons (104). DEGs were identified with a false discovery rate (Benjamini-Hochberg method) adjusted *p*-value <0.05. DEGs with a log2 fold change (Log2FC) over 1 and adj. $p < 0.05$ were used for downstream functional analysis in *Experiments 1 to 4*. A fold-change cut-off was not used for *Experiment 5*. Kyoto Encyclopedia of Genes and Genomes and Reactome (https://reactome.org/) were utilized for pathway analysis. We utilized clusterProfiler (Version 4.4.1), ReactomePA, ggplot2 (3.15), and ConcensusPathDB (105) with mouse as the reference organism.

Digital cell sorting with CIBERSORTx

CIBERSORTx (https://cibersortx.stanford.edu/) is a machine learning method that enables prediction of cell type proportions from bulk tissue analysis using single cell RNA-seq data (42). We used skeletal muscle single-cell data from 10 days muscle regeneration data from Oprescu *et al.* (43). The datasets (10X Genomics) were reanalyzed with Seurat, and cell clusters were identified with a resolution of 0.8 (106). Normalized gene expression matrices of individual cells were used to create a signature matrix of all cell types using default settings, and cell proportions were predicted by CIBERSORTx with 1000 permutations.

Transcriptional regulator analysis using Lisa

Lisa was run according to recommended procedures (37). In brief, DEG lists (adj. $p < 0.05$) from *Experiments 4* and *5* were input into the online graphical user interface. Output files were downloaded and the strength of MYC regulation was determined by ranking of regulatory potential in H3k27ac ChIP-seq files. The Cauchy combination *p*-value test was used to determine overall influence of MYC.

Data availability

Raw data are available in Gene Expression Omnibus GEO213406, and all processed data are provided in Supporting information and online webtools.

Abbreviations—The abbreviations used are: ChIP-seq, chromatin immunoprecipitation sequencing; DEG, differentially expressed gene; ECM, extracellular matrix; EU, 5-Ethenyl uridine; FANS, fluorescent activated nuclear-sorting; Lisa, Landscape *In Silico* deletion analysis; RNA-seq, RNA-sequencing.

References

1. Santoro, A., Vlachou, T., Luzi, L., Melloni, G., Mazzarella, L., D'Elia, E., *et al.* (2019) p53 loss in breast cancer leads to Myc activation, increased cell plasticity, and expression of a mitotic signature with prognostic value. *Cell Rep.* **26**, 624–638.e8
2. Hurlin, P. J. (2013) Control of vertebrate development by MYC. *Cold Spring Harb. Perspect. Med.* **3**, a014332
3. Brenner, C., Deplus, R., Didelot, C., Loriot, A., Viré, E., De Smet, C., *et al.* (2005) Myc represses transcription through recruitment of DNA methyltransferase corepressor. *EMBO J.* **24**, 336–346
4. Lin, C.-H., Lin, C., Tanaka, H., Fero, M. L., and Eisenman, R. N. (2009) Gene regulation and epigenetic remodeling in murine embryonic stem cells by c-Myc. *PLoS One* **4**, e7839
5. Takahashi, K., and Yamanaka, S. (2006) Induction of pluripotent stem cells from mouse embryonic and adult fibroblast cultures by defined factors. *Cell* **126**, 663–676
6. Nakagawa, M., Takizawa, N., Narita, M., Ichisaka, T., and Yamanaka, S. (2010) Promotion of direct reprogramming by transformation-deficient Myc. *Proc. Nat. Acad. Sci. U. S. A.* **107**, 14152–14157
7. Kim, S., Li, Q., Dang, C. V., and Lee, L. A. (2000) Induction of ribosomal genes and hepatocyte hypertrophy by adenovirus-mediated expression of c-Myc *in vivo. Proc. Nat. Acad. Sci. U. S. A.* **97**, 11198–11202
8. Dang, C. V. (2012) MYC on the path to cancer. *Cell* **149**, 22–35
9. Gabay, M., Li, Y., and Felsher, D. W. (2014) MYC activation is a hallmark of cancer initiation and maintenance. *Cold Spring Harb. Perspect. Med.* **4**, a014241
10. Kalkat, M., Wasylishen, A. R., Kim, S. S., and Penn, L. (2011) More than MAX: discovering the Myc interactome. *Cell Cycle* **10**, 374–375
11. Conacci-Sorrell, M., McFerrin, L., and Eisenman, R. N. (2014) An overview of MYC and its interactome. *Cold Spring Harb. Perspect. Med.* **4**, a014357
12. Nie, Z., Hu, G., Wei, G., Cui, K., Yamane, A., Resch, W., *et al.* (2012) c-Myc is a universal amplifier of expressed genes in lymphocytes and embryonic stem cells. *Cell* **151**, 68–79
13. Nie, Z., Guo, C., Das, S. K., Chow, C. C., Batchelor, E., Jnr, S. S. S., *et al.* (2020) Dissecting transcriptional amplification by MYC. *Elife* **9**, e52483
14. Das, S. K., Lewis, B. A., and Levens, D. (2022) MYC: a complex problem. *Trends Cell Biol.* https://doi.org/10.1016/j.tcb.2022.1007.1006
15. Alway, S. E. (1997) Overload-induced C-Myc oncoprotein is reduced in aged skeletal muscle. *J. Gerontol. Ser. A Biol. Sci. Med. Sci.* **52**, B203–B211
16. Whitelaw, P. F., and Hesketh, J. E. (1992) Expression of c-myc and c-fos in rat skeletal muscle. Evidence for increased levels of c-myc mRNA during hypertrophy. *Biochem. J.* **281**, 143–147
17. Chen, Y. W., Nader, G. A., Baar, K. R., Fedele, M. J., Hoffman, E. P., and Esser, K. A. (2002) Response of rat muscle to acute resistance exercise defined by transcriptional and translational profiling. *J. Physiol.* **545**, 27–41
18. Gohil, K., and Brooks, G. A. (2012) Exercise tames the wild side of the Myc network: a hypothesis. *Am. J. Physiol. Endocrinol. Metab.* **303**, E18–E30
19. von Walden, F., Rea, M., Mobley, C. B., Fondufe-Mittendorf, Y., McCarthy, J. J., Peterson, C. A., *et al.* (2020) The myonuclear DNA methylome in response to an acute hypertrophic stimulus. *Epigenetics* **15**, 1151–1162
20. von Walden, F., Casagrande, V., Östlund Farrants, A.-K., and Nader, G. A. (2012) Mechanical loading induces the expression of a Pol I regulon at the onset of skeletal muscle hypertrophy. *Am. J. Physiol. Cell Physiol.* **302**, C1523–C1530
21. Mori, T., Ato, S., Knudsen, J. R., Henriquez-Olguin, C., Li, Z., Wakabayashi, K., *et al.* (2020) c-Myc overexpression increases ribosome biogenesis and protein synthesis independent of mTORC1 activation in mouse skeletal muscle. *Am. J. Physiol. Endocrinol. Metab.* **321**, E551–E559
22. West, D. W., Baehr, L. M., Marcotte, G. R., Chason, C. M., Tolento, L., Gomes, A. V., *et al.* (2016) Acute resistance exercise activates rapamycin-sensitive and -insensitive mechanisms that control translational activity and capacity in skeletal muscle. *J. Physiol.* **594**, 453–468
23. Figueiredo, V. C., Wen, Y., Alkner, B., Fernandez-Gonzalo, R., Norrbom, J., Vechetti, I. J., Jr., *et al.* (2021) Genetic and epigenetic regulation of skeletal muscle ribosome biogenesis with exercise. *J. Physiol.* **599**, 3363–3384
24. Felsher, D. W., and Bishop, J. M. (1999) Transient excess of MYC activity can elicit genomic instability and tumorigenesis. *Proc. Nat. Acad. Sci. U. S. A.* **96**, 3940
25. Kirby, T. J., Patel, R. M., McClintock, T. S., Dupont-Versteegden, E. E., Peterson, C. A., and McCarthy, J. J. (2016) Myonuclear transcription is responsive to mechanical load and DNA content but uncoupled from cell size during hypertrophy. *Mol. Biol. Cell* **27**, 788–798
26. Chaillou, T., Lee, J. D., England, J. H., Esser, K. A., and McCarthy, J. J. (2013) Time course of gene expression during mouse skeletal muscle hypertrophy. *J. Appl. Physiol.* **115**, 1065–1074
27. Armstrong, D. D., and Esser, K. A. (2005) Wnt/β-catenin signaling activates growth-control genes during overload-induced skeletal muscle hypertrophy. *Am. J. Physiol. Cell Physiol.* **289**, C853–C859
28. Goodman, C. A., Dietz, J. M., Jacobs, B. L., McNally, R. M., You, J.-S., and Hornberger, T. A. (2015) Yes-associated protein is up-regulated by mechanical overload and is sufficient to induce skeletal muscle hypertrophy. *FEBS Lett.* **589**, 1491–1497
29. Stec, M. J., Kelly, N. A., Many, G. M., Windham, S. T., Tuggle, S. C., and Bamman, M. M. (2016) Ribosome biogenesis may augment resistance training-induced myofiber hypertrophy and is required for myotube growth *in vitro. Am. J. Physiol. Endocrinol. Metab.* **310**, E652–E661
30. Seely, S. (1980) Possible reasons for the high resistance of muscle to cancer. *Med. Hypotheses* **6**, 133–137
31. Keckesova, Z., Donaher, J. L., De Cock, J., Freinkman, E., Lingrell, S., Bachovchin, D. A., *et al.* (2017) LACTB is a tumour suppressor that modulates lipid metabolism and cell state. *Nature* **543**, 681–686
32. Sridhar, K. S., Rao, R. K., and Kunhardt, B. (1987) Skeletal muscle metastases from lung cancer. *Cancer* **59**, 1530–1534
33. Crist, S. B., Nemkov, T., Dumpit, R. F., Dai, J., Tapscott, S. J., True, L. D., *et al.* (2022) Unchecked oxidative stress in skeletal muscle prevents outgrowth of disseminated tumour cells. *Nat. Cell Biol.* **24**, 1–16
34. Kirby, T. J., McCarthy, J. J., Peterson, C. A., and Fry, C. S. (2016) Synergist ablation as a rodent model to study satellite cell dynamics in adult skeletal muscle. *Methods Mol. Biol.* **1460**, 43–52
35. Murach, K. A., McCarthy, J. J., Peterson, C. A., and Dungan, C. M. (2020) Making mice mighty: recent advances in translational models of load-induced muscle hypertrophy. *J. Appl. Physiol.* **129**, 516–521
36. Figueiredo, V. C., Roberts, L. A., Markworth, J. F., Barnett, M. P. G., Coombes, J. S., Raastad, T., *et al.* (2016) Impact of resistance exercise on ribosome biogenesis is acutely regulated by post-exercise recovery strategies. *Physiol. Rep.* **4**, e12670
37. Qin, Q., Fan, J., Zheng, R., Wan, C., Mei, S., Wu, Q., *et al.* (2020) Lisa: inferring transcriptional regulators through integrative modeling of public chromatin accessibility and ChIP-seq data. *Genome Biol.* **21**, 32

38. Valentino, T., Figueiredo, V. C., Mobley, C. B., McCarthy, J. J., and Vechetti, I. J., Jr. (2021) Evidence of myomiR regulation of the pentose phosphate pathway during mechanical load-induced hypertrophy. *Physiol. Rep.* **9**, e15137

39. Wackerhage, H., Vechetti, I. J., Baumert, P., Gehlert, S., Becker, L., Jaspers, R. T., *et al.* (2022) Does a hypertrophying muscle fibre reprogramme its metabolism similar to a cancer cell? *Sport Med.* https://doi.org/10.1007/s40279-022-01676-1

40. Verbrugge, S. A., Gehlert, S., Stadhouders, L. E., Jacko, D., Aussieker, T., MJ de Wit, G., *et al.* (2020) PKM2 determines myofiber hypertrophy *in vitro* and increases in response to resistance exercise in human skeletal muscle. *Int. J. Mol. Sci.* **21**, 7062

41. Vazquez, A., Liu, J., Zhou, Y., and Oltvai, Z. N. (2010) Catabolic efficiency of aerobic glycolysis: the Warburg effect revisited. *BMC Syst. Biol.* **4**, 1–9

42. Newman, A. M., Steen, C. B., Liu, C. L., Gentles, A. J., Chaudhuri, A. A., Scherer, F., *et al.* (2019) Determining cell type abundance and expression from bulk tissues with digital cytometry. *Nat. Biotech.* **37**, 773–782

43. Oprescu, S. N., Yue, F., Qiu, J., Brito, L. F., and Kuang, S. (2020) Temporal dynamics and heterogeneity of cell populations during skeletal muscle regeneration. *iScience* **23**, 100993

44. Murach, K. A., Peck, B. D., Policastro, R. A., Vechetti, I. J., Van Pelt, D. W., Dungan, C. M., *et al.* (2021) Early satellite cell communication creates a permissive environment for long-term muscle growth. *iScience* **24**, 102372

45. Fry, C. S., Kirby, T. J., Kosmac, K., McCarthy, J. J., and Peterson, C. A. (2017) Myogenic progenitor cells control extracellular matrix production by fibroblasts during skeletal muscle hypertrophy. *Cell Stem Cell* **20**, 56–69

46. Zak, R., Rabinowitz, M., and Platt, C. (1967) Ribonucleic acids associated with myofibrils. *Biochemistry* **6**, 2493–2500

47. Rodríguez-Fdez, S., and Bustelo, X. R. (2021) Rho GTPases in skeletal muscle development and homeostasis. *Cells* **10**, 2984

48. Ohsawa, I., and Kawano, F. (2021) Chronic exercise training activates histone turnover in mouse skeletal muscle fibers. *FASEB J.* **35**, e21453

49. Murach, K. A., Dungan, C. M., von Walden, F., and Wen, Y. (2021) Epigenetic evidence for distinct contributions of resident and acquired myonuclei during long-term exercise adaptation using timed *in vivo* myonuclear labeling. *Am. J. Physiol. Cell Physiol.* **32**, C86–C93

50. Lin, J., Wu, H., Tarr, P. T., Zhang, C.-Y., Wu, Z., Boss, O., *et al.* (2002) Transcriptional co-activator PGC-1α drives the formation of slow-twitch muscle fibres. *Nature* **418**, 797–801

51. Puigserver, P., Wu, Z., Park, C. W., Graves, R., Wright, M., and Spiegelman, B. M. (1998) A cold-inducible coactivator of nuclear receptors linked to adaptive thermogenesis. *Cell* **92**, 829–839

52. Iwata, M., Englund, D. A., Wen, Y., Dungan, C. M., Murach, K. A., Vechetti, I. J., *et al.* (2018) A novel tetracycline-responsive transgenic mouse strain for skeletal muscle-specific gene expression. *Skelet Muscle* **8**, 33

53. Murach, K. A., Vechetti, I. J., Jr., Van Pelt, D. W., Crow, S. E., Dungan, C. M., Figueiredo, V. C., *et al.* (2020) Fusion-independent satellite cell communication to muscle fibers during load-induced hypertrophy. *Function (Oxf.)* **1**, zqaa009

54. Player, D., Martin, N., Passey, S., Sharples, A., Mudera, V., and Lewis, M. (2014) Acute mechanical overload increases IGF-I and MMP-9 mRNA in 3D tissue-engineered skeletal muscle. *Biotech. Lett.* **36**, 1113–1124

55. Dahiya, S., Bhatnagar, S., Hindi, S. M., Jiang, C., Paul, P. K., Kuang, S., *et al.* (2011) Elevated levels of active matrix metalloproteinase-9 cause hypertrophy in skeletal muscle of normal and dystrophin-deficient mdx mice. *Hum. Mol Genet.* **20**, 4345–4359

56. Accornero, F., Kanisicak, O., Tjondrokoesoemo, A., Attia, A. C., McNally, E. M., and Molkentin, J. D. (2014) Myofiber-specific inhibition of TGFβ signaling protects skeletal muscle from injury and dystrophic disease in mice. *Hum. Mol Genet.* **23**, 6903–6915

57. Petrosino, J. M., Leask, A., and Accornero, F. (2019) Genetic manipulation of CCN2/CTGF unveils cell-specific ECM-remodeling effects in injured skeletal muscle. *FASEB J.* **33**, 2047–2057

58. Brightwell, C. R., Latham, C. M., Thomas, N. T., Keeble, A. R., Murach, K. A., and Fry, C. S. (2022) A glitch in the matrix: the pivotal role for extracellular matrix remodeling during muscle hypertrophy. *Am. J. Physiol. Cell Physiol.* https://doi.org/10.1152/ajpcell.00200.02022

59. Wang, X., Blagden, C., Fan, J., Nowak, S. J., Taniuchi, I., Littman, D. R., *et al.* (2005) Runx1 prevents wasting, myofibrillar disorganization, and autophagy of skeletal muscle. *Genes Dev.* **19**, 1715–1722

60. Agrawal, P., Yu, K., Salomon, A. R., and Sedivy, J. M. (2010) Proteomic profiling of Myc-associated proteins. *Cell Cycle* **9**, 4908–4921

61. Pippa, R., Dominguez, A., Malumbres, R., Endo, A., Arriazu, E., Marcotegui, N., *et al.* (2017) MYC-dependent recruitment of RUNX1 and GATA2 on the SET oncogene promoter enhances PP2A inactivation in acute myeloid leukemia. *Oncotarget* **8**, 53989

62. Petrany, M. J., Swoboda, C. O., Sun, C., Chetal, K., Chen, X., Weirauch, M. T., *et al.* (2020) Single-nucleus RNA-seq identifies transcriptional heterogeneity in multinucleated skeletal myofibers. *Nat. Commun.* **11**, 1–12

63. Barash, I. A., Mathew, L., Ryan, A. F., Chen, J., and Lieber, R. L. (2004) Rapid muscle-specific gene expression changes after a single bout of eccentric contractions in the mouse. *Am. J. Physiol. Cell Physiol.* **286**, C355–C364

64. Mahoney, D. J., Safdar, A., Parise, G., Melov, S., Fu, M., MacNeil, L., *et al.* (2008) Gene expression profiling in human skeletal muscle during recovery from eccentric exercise. *Am. J. Physiol. Regul. Integr. Comp. Physiol.* **294**, R1901–R1910

65. Armstrong, R., Marum, P., Tullson, P., and Saubert, C., 4th (1979) Acute hypertrophic response of skeletal muscle to removal of synergists. *J. Appl. Physiol.* **46**, 835–842

66. Chaillou, T. (2019) Ribosome specialization and its potential role in the control of protein translation and skeletal muscle size. *J. Appl. Physiol.* **127**, 599–607

67. Strezoska, Z. A., Pestov, D. G., and Lau, L. F. (2000) Bop1 is a mouse WD40 repeat nucleolar protein involved in 28S and 5.8 S rRNA processing and 60S ribosome biogenesis. *Mol. Cell. Biol.* **20**, 5516–5528

68. Lapik, Y. R., Fernandes, C. J., Lau, L. F., and Pestov, D. G. (2004) Physical and functional interaction between Pes1 and Bop1 in mammalian ribosome biogenesis. *Mol. Cell* **15**, 17–29

69. Morello, L. G., Coltri, P. P., Quaresma, A. J., Simabuco, F. M., Silva, T. C., Singh, G., *et al.* (2011) The human nucleolar protein FTSJ3 associates with NIP7 and functions in pre-rRNA processing. *PLoS One* **6**, e29174

70. Madan, B., Harmston, N., Nallan, G., Montoya, A., Faull, P., Petretto, E., *et al.* (2019) Temporal dynamics of Wnt-dependent transcriptome reveal an oncogenic Wnt/MYC/ribosome axis. *J. Clin. Invest.* **128**, 5620–5633

71. Wang, H., Wang, L., Wang, Z., Dang, Y., Shi, Y., Zhao, P., *et al.* (2020) The nucleolar protein NOP2 is required for nucleolar maturation and ribosome biogenesis during preimplantation development in mammals. *FASEB J.* **34**, 2715–2729

72. Idol, R. A., Robledo, S., Du, H.-Y., Crimmins, D. L., Wilson, D. B., Ladenson, J. H., *et al.* (2007) Cells depleted for RPS19, a protein associated with Diamond Blackfan Anemia, show defects in 18S ribosomal RNA synthesis and small ribosomal subunit production. *Blood Cell Mol. Dis.* **39**, 35–43

73. O'Donnell, K. A., Wentzel, E. A., Zeller, K. I., Dang, C. V., and Mendell, J. T. (2005) c-Myc-regulated microRNAs modulate E2F1 expression. *Nature* **435**, 839–843

74. Wang, X., Zhao, X., Gao, P., and Wu, M. (2013) c-Myc modulates microRNA processing via the transcriptional regulation of Drosha. *Sci. Rep.* **3**, 1–7

75. Lin, C. H., Jackson, A. L., Guo, J., Linsley, P. S., and Eisenman, R. N. (2009) Myc-regulated microRNAs attenuate embryonic stem cell differentiation. *EMBO J.* **28**, 3157–3170

76. Bui, T. V., and Mendell, J. T. (2010) Myc: maestro of microRNAs. *Genes Cancer* **1**, 568–575

77. Luo, W., Chen, J., Li, L., Ren, X., Cheng, T., Lu, S., *et al.* (2019) c-Myc inhibits myoblast differentiation and promotes myoblast proliferation and muscle fibre hypertrophy by regulating the expression of its target genes, miRNAs and lincRNAs. *Cell Death Differ.* **26**, 426–442

78. Bloemberg, D., and Quadrilatero, J. (2012) Rapid determination of myosin heavy chain expression in rat, mouse, and human skeletal muscle using multicolor immunofluorescence analysis. *PLoS One* **7**, e35273

79. Dungan, C. M., Brightwell, C., Wen, Y., Zdunek, C. J., Latham, C., Thomas, N. T., *et al.* (2022) Muscle-specific cellular and molecular adaptations to late-life voluntary concurrent exercise. *Function (Oxf.)* **3**, zqac027

80. Altman, B. J., Hsieh, A. L., Sengupta, A., Krishnanaiah, S. Y., Stine, Z. E., Walton, Z. E., *et al.* (2015) MYC disrupts the circadian clock and metabolism in cancer cells. *Cell Metab.* **22**, 1009–1019

81. Shostak, A., Ruppert, B., Ha, N., Bruns, P., Toprak, U. H., Eils, R., *et al.* (2016) MYC/MIZ1-dependent gene repression inversely coordinates the circadian clock with cell cycle and proliferation. *Nat. Commun.* **7**, 1–11

82. Li, Z., Ivanov, A. A., Su, R., Gonzalez-Pecchi, V., Qi, Q., Liu, S., *et al.* (2017) The OncoPPi network of cancer-focused protein–protein interactions to inform biological insights and therapeutic strategies. *Nat. Commun.* **8**, 1–14

83. Cai, X., Gao, L., Teng, L., Ge, J., Oo, Z. M., Kumar, A. R., *et al.* (2015) Runx1 deficiency decreases ribosome biogenesis and confers stress resistance to hematopoietic stem and progenitor cells. *Cell Stem Cell* **17**, 165–177

84. Nishikawa, K., Lindstedt, S. L., Hessel, A., and Mishra, D. (2020) N2A titin: signaling hub and mechanical switch in skeletal muscle. *Int. J. Mol. Sci.* **21**, 3974

85. van der Pijl, R. J., Domenighetti, A. A., Sheikh, F., Ehler, E., Ottenheijm, C. A., and Lange, S. (2021) The titin N2B and N2A regions: biomechanical and metabolic signaling hubs in cross-striated muscles. *Biophys. Rev.* **13**, 653–677

86. van der Pijl, R. J., van den Berg, M., van de Locht, M., Shen, S., Bogaards, S. J., Conijn, S., *et al.* (2021) Muscle ankyrin repeat protein 1 (MARP1) locks titin to the sarcomeric thin filament and is a passive force regulator. *J. Gen. Physiol.* **153**, e202112925

87. Liu, X.-H., Bauman, W. A., and Cardozo, C. (2015) ANKRD1 modulates inflammatory responses in C2C12 myoblasts through feedback inhibition of NF-κB signaling activity. *Biochem. Biophys. Res. Commun.* **464**, 208–213

88. Wu, Y., Ruggiero, C. L., Bauman, W. A., and Cardozo, C. (2013) Ankrd1 is a transcriptional repressor for the androgen receptor that is downregulated by testosterone. *Biochem. Biophys. Res. Commun.* **437**, 355–360

89. Zambon, A. C., McDearmon, E. L., Salomonis, N., Vranizan, K. M., Johansen, K. L., Adey, D., *et al.* (2003) Time-and exercise-dependent gene regulation in human skeletal muscle. *Genome Biol.* **4**, 1–12

90. Wolff, G., and Esser, K. A. (2012) Scheduled exercise phase shifts the circadian clock in skeletal muscle. *Med. Sci. Sport Exerc.* **44**, 1663

91. Casanova-Vallve, N., Duglan, D., Vaughan, M. E., Pariollaud, M., Handzlik, M. K., Fan, W., *et al.* (2022) Daily running enhances molecular and physiological circadian rhythms in skeletal muscle. *Mol. Metab.* **61**, 101504

92. Small, L., Altıntaş, A., Laker, R. C., Ehrlich, A., Pattamaprapanont, P., Villarroel, J., *et al.* (2020) Contraction influences Per2 gene expression in skeletal muscle through a calcium-dependent pathway. *J. Physiol.* **598**, 5739–5752

93. Gerst, J. E. (2018) Pimp my ribosome: ribosomal protein paralogs specify translational control. *Trend Genet.* **34**, 832–845

94. Kirby, T. J., Lee, J. D., England, J. H., Chaillou, T., Esser, K. A., and McCarthy, J. J. (2015) Blunted hypertrophic response in aged skeletal muscle is associated with decreased ribosome biogenesis. *J. Appl. Physiol.* **119**, 321–327

95. Wen, Y., Alimov, A. P., and McCarthy, J. J. (2016) Ribosome biogenesis is necessary for skeletal muscle hypertrophy. *Exerc. Sport Sci. Rev.* **44**, 110

96. von Walden, F. (2019) Ribosome biogenesis in skeletal muscle: coordination of transcription and translation. *J. Appl. Physiol.* **127**, 591–598

97. Figueiredo, V. C., and McCarthy, J. J. (2018) Regulation of ribosome biogenesis in skeletal muscle hypertrophy. *Physiology* **34**, 30–42

98. Fry, C. S., Lee, J. D., Jackson, J. R., Kirby, T. J., Stasko, S. A., Liu, H., *et al.* (2014) Regulation of the muscle fiber microenvironment by activated satellite cells during hypertrophy. *FASEB J.* **28**, 1654–1665

99. DePinho, R., Mitsock, L., Hatton, K., Ferrier, P., Zimmerman, K., Legouy, E., *et al.* (1987) Myc family of cellular oncogenes. *J. Cell Biochem.* **33**, 257–266

100. Tumbar, T., Guasch, G., Greco, V., Blanpain, C., Lowry, W. E., Rendl, M., *et al.* (2004) Defining the epithelial stem cell niche in skin. *Science* **303**, 359–363

101. Felsher, D. W., and Bishop, J. M. (1999) Reversible tumorigenesis by MYC in hematopoietic lineages. *Mol. Cell* **4**, 199–207

102. Rutledge, E. A., Lindström, N. O., Michos, O., and McMahon, A. P. (2020) Genetic manipulation of ureteric bud tip progenitors in the mammalian kidney through an Adamts18 enhancer driven tet-on inducible system. *Dev. Biol.* **458**, 164–176

103. Wen, Y., Dungan, C. M., Mobley, C. B., Valentino, T., von Walden, F., and Murach, K. A. (2021) Nucleus type-specific DNA methylomics reveals epigenetic "memory" of prior adaptation in skeletal muscle. *Function (Oxf.)* **2**, zqab038

104. Love, M. I., Huber, W., and Anders, S. (2014) Moderated estimation of fold change and dispersion for RNA-seq data with DESeq2. *Genome Biol.* **15**, 550

105. Kamburov, A., and Herwig, R. (2022) ConsensusPathDB 2022: molecular interactions update as a resource for network biology. *Nucleic Acid Res.* **50**, D587–D595

106. Hao, Y., Hao, S., Andersen-Nissen, E., Mauck, W. M., III, Zheng, S., Butler, A., *et al.* (2021) Integrated analysis of multimodal single-cell data. *Cell* **184**, 3573–3587.e29